Metal-Oxo Clusters Hot Paper

How to cite: *Angew. Chem. Int. Ed.* **2022,** *61,* e202203114
International Edition: doi.org/10.1002/anie.202203114
German Edition: doi.org/10.1002/ange.202203114

Discrete, Cationic Palladium(II)-Oxo Clusters via f-Metal Ion Incorporation and their Macrocyclic Host-Guest Interactions with Sulfonatocalixarenes

*Saurav Bhattacharya, Andrea Barba-Bon, Tsedenia A. Zewdie, Anja B. Müller, Talha Nisar, Anna Chmielnicka, Iwona A. Rutkowska, Christian J. Schürmann, Veit Wagner, Nikolai Kuhnert, Pawel J. Kulesza, Werner M. Nau, and Ulrich Kortz**

Dedicated to Professor Michael T. Pope on the occasion of his 89th birthday

Abstract: We report on the discovery of the first two examples of cationic palladium(II)-oxo clusters (POCs) containing *f*-metal ions, $[Pd^{II}_6O_{12}M_8\{(CH_3)_2AsO_2\}_{16}(H_2O)_8]^{4+}$ ($M=Ce^{IV}$, Th^{IV}), and their physicochemical characterization in the solid state, in solution and in the gas phase. The molecular structure of the two novel POCs comprises an octahedral $\{Pd_6O_{12}\}^{12-}$ core that is capped by eight M^{IV} ions, resulting in a cationic, cubic assembly $\{Pd_6O_{12}M^{IV}_8\}^{20+}$, which is coordinated by a total of 16 terminal dimethylarsinate and eight water ligands, resulting in the mixed Pd^{II}-Ce^{IV}/Th^{IV} oxo-clusters $[Pd^{II}_6O_{12}M_8\{(CH_3)_2AsO_2\}_{16}(H_2O)_8]^{4+}$ ($M=Ce$, **Pd_6Ce_8**; Th, **Pd_6Th_8**). We have also studied the formation of host-guest inclusion complexes of **Pd_6Ce_8** and **Pd_6Th_8** with anionic 4-sulfocalix[*n*]arenes ($n=4$, 6, 8), resulting in the first examples of discrete, enthalpically-driven supramolecular assemblies between large metal-oxo clusters and calixarene-based macrocycles. The POCs were also found to be useful as pre-catalysts for electrocatalytic CO_2-reduction and HCOOH-oxidation.

Introduction

Metal-oxo clusters, which can be considered to be a subset of coordination cage complexes, are constructed by linking metal ions with oxygen-based ligands, such as oxo, hydroxo or aqua. This leads to discrete molecular units that possess well-defined structures and formulae. By subtle variation of the reaction medium pH, temperature, metal ion type and concentration, ionic strength, redox environment, and the terminating capping groups, it is possible to control the extent of hydrolysis and condensation, and hence the shape, size and composition of the resulting metal-oxo clusters.[1] Several transition metal- and lanthanide-oxo/hydroxo clusters have been discovered till date,[2] which have shown immense potential in the areas of photocatalytic water oxidation,[3] single-molecular magnetism and cryogenic magnetic cooling devices,[4] as well as band-gap tuning.[5] Furthermore, by utilizing suitable inorganic and/or organic linkers, these metal-oxo clusters can be supramolecularly organized in three dimensions leading to inorganic or metal-organic open-framework materials,[6] which have found use in the areas of organocatalysis, electro- or photocatalysis as well as gas-separation and storage.[6]

One of the most widely studied subclasses of metal-oxo clusters are the anionic polyoxometalates (POMs), which are constructed from early transition metal ions in high oxidation states, such as Mo^{VI}, W^{VI}, V^{V}, Nb^{V}, and Ta^{V} with oxo-linkers, resulting in a large class of compounds with an enormous variety of shapes, sizes and compositions.[7] The high thermal, electrochemical, and photochemical stability of POMs renders them immensely useful in the areas of magnetism, molecular electronics and catalysis.[8] The quest for the realization of purely noble-metal-based oxo-clusters that could potentially be utilized as structural models to better understand noble-metal-based catalysis got its first impetus when, in 2004, the first polyoxoplatinate(III), $[Pt^{III}_{12}O_8(SO_4)_{12}]^{4-}$, was discovered.[9,10a] This was followed, in 2008 and 2010, by the discovery of the first

[*] S. Bhattacharya, A. Barba-Bon, T. A. Zewdie, A. B. Müller, N. Kuhnert, W. M. Nau, U. Kortz
Department of Life Sciences and Chemistry, Jacobs University
Campus Ring 1, 28759 Bremen (Germany)
E-mail: u.kortz@jacobs-university.de

T. Nisar, V. Wagner
Department of Physics and Earth Sciences, Jacobs University
Campus Ring 1, 28759 Bremen (Germany)

A. Chmielnicka, I. A. Rutkowska, P. J. Kulesza
Faculty of Chemistry, University of Warsaw
Pasteura 1, 02-093 Warsaw (Poland)

C. J. Schürmann
Rigaku Europe SE
Hugenottenallee 167, 63263 Neu-Isenburg (Germany)

© 2022 The Authors. Angewandte Chemie International Edition published by Wiley-VCH GmbH. This is an open access article under the terms of the Creative Commons Attribution Non-Commercial NoDerivs License, which permits use and distribution in any medium, provided the original work is properly cited, the use is non-commercial and no modifications or adaptations are made.

© 2022 The Authors. Angewandte Chemie International Edition published by Wiley-VCH GmbH

polyoxopalladate(II) (POP), $[Pd^{II}_{13}As_8O_{34}(OH)_6]^{8-}$,[10b] and the first polyoxoaurate(III), $[Au^{III}_4As_4O_{20}]^{8-}$,[10c] which paved the way for a multitude of other composition, size, and shape-modulated noble-metal ion-based oxo-clusters.[10–14] Most of the reported noble-metal ion-based oxo-clusters are anionic, with very few examples of neutral or cationic clusters none of which, hitherto, were based on palladium.[14] Very recently, the first discrete and neutral palladium-based oxo-clusters were reported, the disk-shaped $[Pd_{16}O_8(OH)_8\{(CH_3)_2AsO_2\}_8]$ (**Pd_{16}**) and its chloro-derivative $[Pd_{16}Na_2O_{10}(OH)_3Cl_3\{(CH_3)_2AsO_2\}_8]$ (**$Pd_{16}Cl$**), the doubly-capped disk $[Pd_{24}O_{12}(OH)_8\{(CH_3)_2AsO_2\}_{16}]$ (**Pd_{24}**), and $[Pd_{40}O_{24}(OH)_{16}\{(CH_3)_2AsO_2\}_{16}]$ (**Pd_{40}**), which is the largest neutral Pd-oxo cluster isolated till date.[15] Herein, we report on the synthesis and structural characterization (solid-state, solution and gaseous-state) of the first two discrete and cationic palladium-oxo clusters (POCs), and their host-guest inclusion complex formation with anionic macrocyclic hosts 4-sulfocalix[*n*]arenes (*n* = 4,6, and 8).

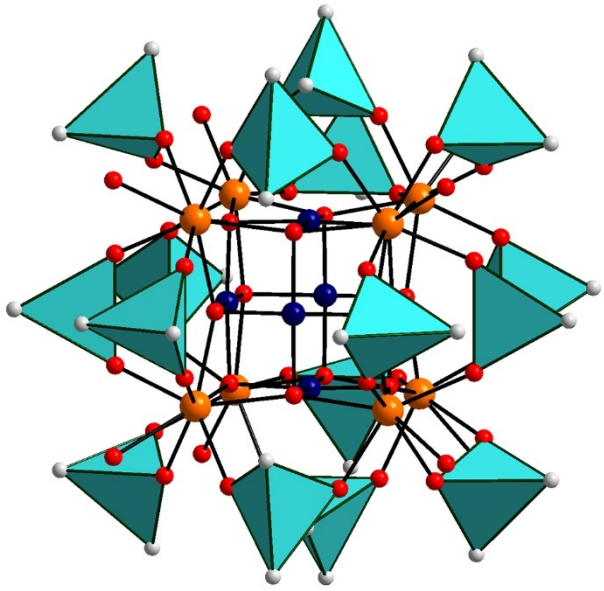

Figure 1. Structural representation of the cationic **Pd_6M_8** oxo-cluster (M = Ce^{IV} or Th^{IV}). Color code: Pd blue, M^{IV} orange, O red, C grey, $(CH_3)_2AsO_2$ cyan tetrahedra.

Results and Discussion

The novel cationic, mixed Pd^{II}-Ce^{IV}/Th^{IV} oxo-clusters $[Pd^{II}_6O_{12}M_8\{(CH_3)_2AsO_2\}_{16}(H_2O)_8]^{4+}$ (M = Ce, **Pd_6Ce_8**; Th, **Pd_6Th_8**) were synthesized by heating mixtures of $PdCl_2$ and $CeCl_3$ for **Pd_6Ce_8** or $Th(NO_3)_4$ for **Pd_6Th_8** in a pH 7 sodium dimethylarsinate (also known as cacodylate) buffer solution at 80 °C for 1 hour, followed by pH adjustment to ≈7 using aq. NaOH solution, and stirring further at 80 °C for 1.5 hours, before filtering and crystallizing (detailed synthetic procedures are given in the Supporting Information). A point to note is that upon addition of γ-cyclodextrin (γ-CD) to the initial reaction mixtures, the reaction proceeded with lesser precipitation, and we obtained a higher yield in both cases. A similar observation was reported recently, wherein the CDs were shown to act as effective co-modulators in the synthesis of the zirconium-oxo cluster-based MOF (UiO-66-NH_2) by facilitating the proper dispersion of the reactants in the aqueous medium by strongly interacting with the hydrophobic organic linkers as well as the metal ions, thereby expediting the coordination of the organic linkers to the metal ions (see Supporting Information).[16]

Single-crystal XRD studies[17] revealed that both **Pd_6Ce_8** and **Pd_6Th_8** crystallize in the orthorhombic space group *Pmmn* (Table S1), and their asymmetric units consist of two Ce^{IV} and Th^{IV} ions, respectively, along with four Pd^{II} ions. Therefore, the molecular clusters are composed of six square-planar coordinated Pd^{II} ions, and eight distorted square-antiprismatic coordinated Ce^{IV} and Th^{IV} ions, respectively, which are connected to each other via 12 μ_4-oxo groups (O1, O2, O3, O4 and O5, see Figure 1). The square-planar coordination environment of the Pd^{II} ions is formed exclusively by the μ_4-oxo groups (Pd–O distances in the range of 2.009(5)–2.038(6) Å for **Pd_6Ce_8** and in the range of 2.019(8)–2.062(9) Å for **Pd_6Th_8**), whereas the distorted square-antiprismatic coordination environment around the Ce^{IV} and Th^{IV} ions is formed by three μ_4-oxo groups, four cacodylate oxygens, and a terminal aqua ligand (Ce–O distances in the range of 2.249(5)–2.664(6) Å and Th–O distances in the range of 2.340(7)–2.674(7) Å, see Tables S2 and S3). Additionally, the molecular structures can be visualized as comprising an octahedral $\{Pd_6O_{12}\}^{12-}$ core that is capped by eight M^{IV} ions resulting in a cationic, cubic assembly $\{Pd_6O_{12}M^{IV}_8\}^{20+}$, which is coordinated by a total of 16 terminal dimethylarsinate and eight water ligands, resulting in the cationic, mixed Pd^{II}-Ce^{IV}/Th^{IV} oxo-clusters $[Pd^{II}_6O_{12}M_8\{(CH_3)_2AsO_2\}_{16}(H_2O)_8]^{4+}$ (M = Ce, **Pd_6Ce_8**; Th, **Pd_6Th_8**), see Figure S1. Therefore, **Pd_6Ce_8** and **Pd_6Th_8** can be considered as discrete molecular equivalents of nano-structured Pd@ceria or Pd@thoria,[18] with the extended three-dimensional structure having been arrested by the cacodylate capping moieties. The structures of CeO_2 and ThO_2 (Figure S2) consist of a face-centered-cubic (*fcc*) arrangement of the Ce^{IV} and Th^{IV} ions, respectively, with all eight tetrahedral holes being filled by oxo anions.[19] In comparison, the discrete molecular structure of **Pd_6M_8** also possesses a *fcc* arrangement of metal ions, the difference being that here the corners of the cube are occupied by Ce^{IV} or Th^{IV} ions, whereas the face-centers are occupied by Pd^{II} ions (Figures 1 and S1). After searching the literature, it became apparent that Ce^{IV}- and Th^{IV}-based oxo-clusters, including cationic species, hade been reported before.[6d, 20] However, **Pd_6Ce_8** and **Pd_6Th_8** are the first palladium-based oxo-clusters of cerium and thorium ever reported. In the solid-state lattice, the cationic **Pd_6M_8** clusters are held together by strong H-bond interactions between the water molecules coordinated to the M^{IV} ions and the lattice water molecules and chloride ions (Tables S4 and S5).

Powder X-ray diffraction (PXRD) studies on **Pd_6Ce_8** and **Pd_6Th_8** indicated that the compounds were crystalline and

© 2022 The Authors. Angewandte Chemie International Edition published by Wiley-VCH GmbH

pure as evidenced from the fact that the PXRD spectra of freshly prepared samples matched well with the simulated PXRD spectra (calculated from the SC-XRD data, see Figure S3). The thermogravimetric analysis (TGA) curves of freshly-prepared **Pd_6Ce_8** and **Pd_6Th_8** between room temperature and 100 °C indicated weight losses of ≈16.3 % and ≈13 %, respectively, which corresponds to the loss of the lattice water molecules (calculated ≈16 % for **Pd_6Ce_8** and ≈14 % for **Pd_6Th_8**, respectively), see Figure S4. The infrared (FT-IR) spectra of **Pd_6Ce_8** and **Pd_6Th_8** indicated the presence of the characteristic bond-stretches corresponding to Pd–O, Ce/Th–O, As–C and C–H (cacodylate moieties) as well as O–H (of H_2O) bonds (see detailed analysis in the Supporting Information, Figure S5). The presence of a nitrate as a counter-anion in **Pd_6Th_8** and its absence in **Pd_6Ce_8** was also confirmed by IR spectroscopy. X-ray photoelectron spectroscopy (XPS) measurements were performed on both **Pd_6Ce_8** and **Pd_6Th_8** in order to ascertain the oxidation states of Pd, Ce and Th. Both **Pd_6Ce_8** and **Pd_6Th_8** exhibited a Pd $3d_{5/2}$ band at ≈337 eV, which is typical for Pd in a 2+ oxidation state (Figure S6a).[21] The XPS spectra of $CeCl_3$ and $(NH_4)_2Ce(NO_3)_6$ as references for Ce^{III} and Ce^{IV}-containing compounds are given in Figure S6b, which exhibit the characteristic multiplet-peaks corresponding to the spin-orbit split $3d_{5/2}$ and $3d_{3/2}$ core holes in the region 880–910 eV.[21d] In addition, the satellite peak at ≈916.5 eV observed for $(NH_4)_2Ce(NO_3)_6$ is characteristic of the presence of Ce^{IV}. This peak was also observed in the XPS spectrum of **Pd_6Ce_8** at ≈916.4 eV, indicating that Ce is in the 4+ oxidation state (Figure S6b). The XPS spectrum of **Pd_6Th_8** exhibited the characteristic $4f_{7/2}$ and $4f_{5/2}$ peaks at ≈344.5 and ≈335.6 eV, respectively, which match well with the XPS spectrum of the $Th(NO_3)_4$ reference (Figure S6a).[21e] These observations were also corroborated by bond valence sum (BVS) calculations on Ce in **Pd_6Ce_8** and Th in **Pd_6Th_8**, which indicated unequivocally that Ce and Th are in the 4+ oxidation state (Tables S6 and S7).

The cationic **Pd_6M_8** oxo-clusters possess idealized C_{2v} point group symmetry with the C_2 principal axis of rotation passing through the Pd^{II} ions Pd1 and Pd3, and the two σ_v planes containing the Pd^{II} ions Pd1, Pd2, and Pd3, as well as Pd1, Pd3, and Pd4, respectively. Consequently, the discrete **Pd_6M_8** oxo-cluster has seven types of structurally inequivalent cacodylate moieties, two each of As1, As2, As3, As5, As6 and As7, and four of As4. This should lead to seven signals in the ^1H and ^{13}C NMR spectra of aqueous solutions of the **Pd_6M_8** oxo-clusters with expected integration ratios of 1:1:1:1:1:1:2. However, the ^1H NMR (D_2O) spectra of both **Pd_6Ce_8** and **Pd_6Th_8** (Figure 2) exhibit five signals, originating from the methyl hydrogens of the cacodylate groups with chemical shift values of 1.48, 1.68, 1.73, 2.07 and 2.93 ppm for **Pd_6Ce_8**, and 1.46, 1.63, 1.67, 1.94 and 2.78 ppm for **Pd_6Th_8**, with the integration ratios for both being 1:2:3:1:1. It seems that the seemingly inequivalent cacodylates As2, As3 and As5 actually appear as one large peak in the ^1H NMR spectra (Figure S1), most likely because the molecular motion in solution renders them equivalent. The ^1H NMR spectrum of **Pd_6Ce_8** and **Pd_6Th_8** remained unchanged even after a week, which indicates the high

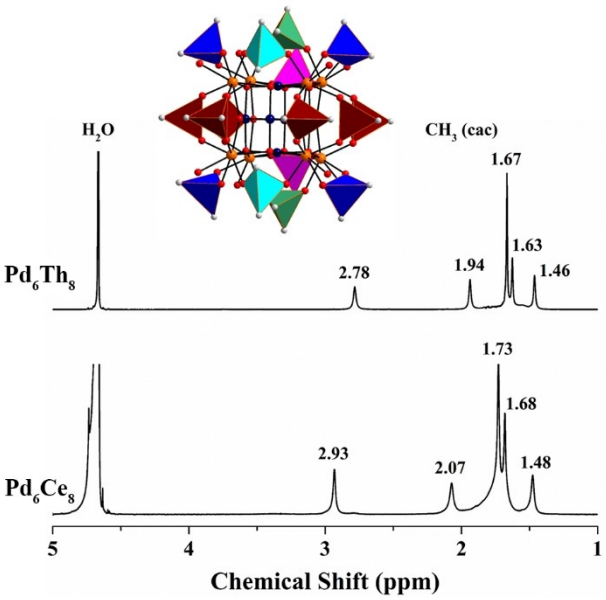

Figure 2. Solution ^1H NMR spectra of **Pd_6Ce_8** and **Pd_6Th_8** in D_2O, inset figure shows the structurally inequivalent cacodylate groups on the cationic oxo-clusters. See text for more details.

solution stability of the two species (Figure S7). In ^{13}C NMR also five signals were observed with chemical shift values of 17.69, 17.86, 18.27, 19.70 and 24.14 ppm for **Pd_6Ce_8**, and 17.69, 17.86, 18.08, 19.30 and 22.76 ppm for **Pd_6Th_8** (Figure S8).

ESI-mass spectra of **Pd_6Th_8** were acquired from aqueous solutions in both positive and negative ion mode. In the negative ion mode, no signals corresponding to the compound were observed. However, in the positive ion mode, two groups of signals centered around *m*/*z* 1219 and 1637 were observed (Figure S9a). As a starting point for spectra assignment, we assumed the presence of the core structure $[Pd^{II}{}_6O_{12}Th_8\{(CH_3)_2AsO_2\}_{16}(H_2O)_8]^{4+}$ (**Pd_6Th_8**) as established by XRD, and the observed isotope pattern is in full agreement with this structure. The signal centered around *m*/*z* 1219 can be assigned to a quadruply-charged species based on the spacing of the isotope peaks. Assuming the absence of the coordinated waters, we observe that the quadruply-charged species $[Pd^{II}{}_6O_{12}Th_8\{(CH_3)_2AsO_2\}_{16}]^{4+}$ is transferred intact into the gas phase (Figure S9b). The simulated mass spectrum is in good agreement with the experimentally observed spectrum. The signal centered at around *m*/*z* 1637 can be assigned to a triply- charged ion accompanied by a chloride anion, reducing the charge of the oxo-cluster from 4+ to 3+ (Figure S9c). For the structural analogue **Pd_6Ce_8**, again no signals were observed in the negative ion mode. However, two signals were observed in the positive ion mode centered at *m*/*z* 2106 and 1381 with isotope patterns expected for the structure (Figure S10a). Following spectral simulations, we assign these signals to a doubly-charged species, $[Pd_6O_{12}Ce_8\{(CH_3)_2AsO_2\}_{16}Cl_2]^{2+}$ (Figure S10b), and to a triply-charged species, $[Pd_6O_{12}\{Ce^{III}Ce^{IV}{}_7\}\{(CH_3)_2AsO_2\}_{16}]^{3+}$ (Figure S10c), where we observe a partial reduction of the Ce^{IV} to Ce^{III} under the

© 2022 The Authors. Angewandte Chemie International Edition published by Wiley-VCH GmbH

ESI-MS conditions. Similar observations have been reported before in the positive ion mode of the ESI-MS spectra of metal complexes.[22]

The formation of host-guest inclusion complexes between inorganic oxo-clusters and organic macrocycles has gained attention only recently, with a focus on the interaction of the clusters with cyclodextrin (CD) macrocycles.[23] Following the initial observation of complex formation between CDs and the Keggin-type POM $[PMo_{12}O_{40}]^{3-}$, different organic-inorganic (CD/POM) systems comprising Wells-Dawson,[24] Keggin,[25] and Lindqvist[25b,26]—type POMs have been reported. Examples of CD complex formation with cationic metal clusters as guests are also known.[24b,27] The superchaotropic nature of the POM anions[28] has been held responsible for their surprisingly strong affinity towards hydrophobic cavities, and the generic driving force has been described as the chaotropic effect, which complements the hydrophobic effect as a new assembly motif in supramolecular chemistry.[29]

This led us to hypothesize that the newly-synthesized cationic mixed-metal oxo-clusters **Pd_6Ce_8** and **Pd_6Th_8** could likewise form supramolecular complexes with organic macrocycles. However, the sizes of the cavities of the CDs (α, β, and γ) span from 6–10 Å,[23b] whereas the size of the **Pd_6M_8** clusters is in the order of ≈15 Å, which excludes the idea of inclusion complexation between the oxo-clusters and the CDs. Indeed, no experimental evidence for interactions between **Pd_6M_8** and CDs was observed. Calixarenes, which are macrocycles containing phenolic moieties linked by methylene bridges at positions 2 and 6 (Figure 3a), play an equally important role in the field of supramolecular chemistry and associated applications.[30] Compared to other macrocyclic hosts, calixarenes do not have a fixed conformation, hence allowing them to also interact with larger guest molecules. Calixarenes display adaptable binding with a preference for inclusion of globular guests.[31] Therefore, we envisaged that calixarenes could be excellent candidates for the formation of supramolecular complexes with the cationic **Pd_6M_8** clusters. As these clusters are positively charged, anionic sulfonatocalixarenes (CX*n*, $n=4$, 6, 8) were expected to interact most strongly, and they were accordingly tested as alternative macrocycles to CDs. CX*n* also have a preference for the desirable conical conformation and all sulfonato groups are ionized near neutral pH.[32]

The complexation of **Pd_6Th_8** with CX4 was evaluated first by a ^{1}H-NMR titration experiment by adding increasing concentrations of **Pd_6Th_8** to a 2 mM CX4 solution in D_2O (Figure 3b). The ^{1}H-NMR peaks of free CX4 are sharp due to a fast conformational cone interconversion, and the bridging methylene protons (axial and equatorial) emerge as a singlet. Upon addition of **Pd_6Th_8**, the methylene singlet peak splits into two broad proton peaks around 4.20 and 3.45 ppm, indicating that the CX4 cavity becomes locked into a cone conformation[33] upon complexation with **Pd_6Th_8**, affording a partial inclusion complex. Surprisingly, the complexation of **Pd_6Ce_8** by CX4 could not be studied by ^{1}H-NMR due to an interference by precipitation at the required mM concentrations.

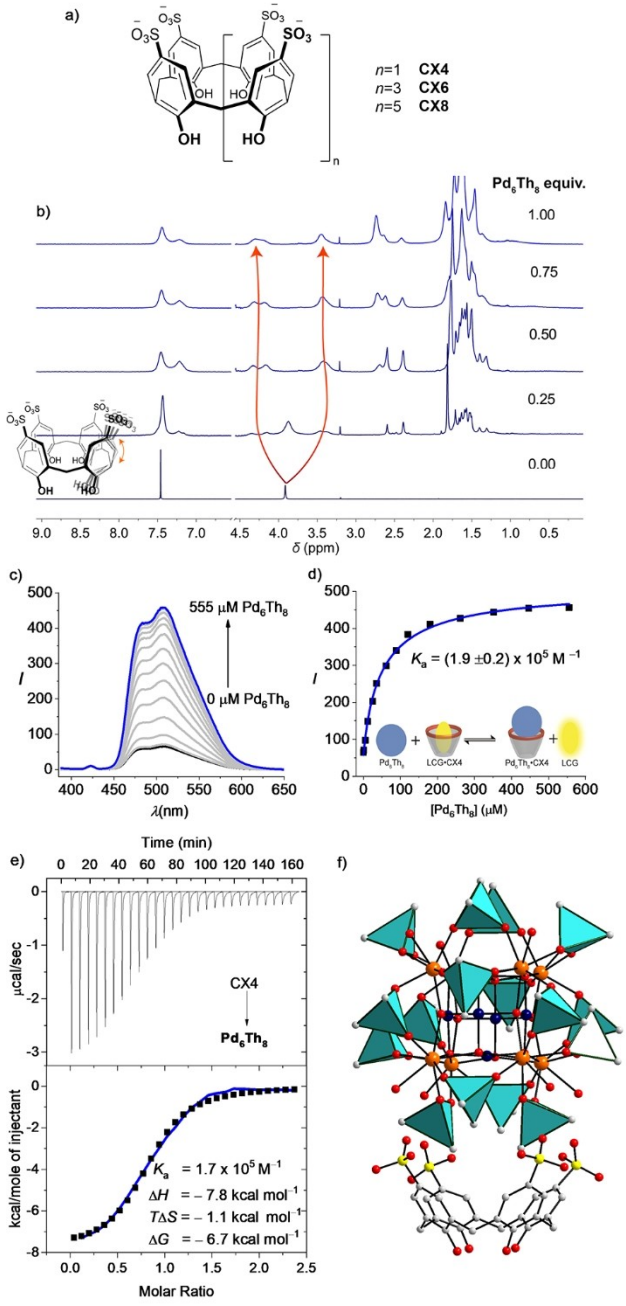

Figure 3. a) Chemical structure of the anionic sulfonatocalixarenes. b) ^{1}H-NMR spectra of CX4 (2 mM) in the presence of increasing **Pd_6Th_8** concentrations. c) Changes in the LCG emission spectra ($\lambda_{ex}=369$ nm), in LCG·CX4 (0.5 μM and 1 μM respectively), upon addition of increasing concentrations of **Pd_6Th_8** (0–555 μM). d) Plot of the maximal fluorescence intensity (from panel c) versus **Pd_6Th_8** concentration, and the corresponding "1host:1guest:1competitor" stoichiometric curve fit; the inset shows the competitive fluorescent indicator principle, where the initial LCG fluorescence is quenched in its CX4 complex (left) and recovered by displacement by the competitive binder (right). e) Microcalorimetric titration of **Pd_6Th_8** by CX4; raw ITC data (top) for sequential injections of CX4 into the **Pd_6Th_8** solution, and apparent reaction heats obtained from the integration of the calorimetric traces with associated fitting to a 1:1 complexation model (bottom). f) SC-XRD structure of the **Pd_6Th_8·CX4** complex. Color code is same as Figure 1 except that sulfurs are represented as light yellow balls.

© 2022 The Authors. Angewandte Chemie International Edition published by Wiley-VCH GmbH

The formation of the **Pd_6Th_8·CX4** complex was further probed by fluorescence titrations by using an indicator displacement assay (IDA),[34] which has been applied in supramolecular chemistry to determine the association constants of optically transparent compounds. Lucigenin (LCG) has been introduced before as ideal fluorescent indicator for CX4;[35] its fluorescence is quenched inside the LCG·CX4 complex, such that the binding by a competitive guest can be followed through a fluorescence increase/recovery. The binding constant of the competitor can be quantified via a fitting of the competitive titration curve. Indeed, the addition of **Pd_6Th_8** (competitive guest) to a quenched solution of LCG·CX4 resulted in an increase of the fluorescence intensity due to dye displacement from CX4 (Figures 3c and d). The binding constant was found to be $(1.9\pm0.2)\times10^5\ M^{-1}$ by using a 1host:1guest:1competitor stoichiometric binding model, which pointed to a strong 1:1 complex formation. The **Pd_6Ce_8** could not be investigated with this method, because the large intrinsic cluster absorbance prevented selective LCG excitation (Figure S11).

ITC titrations were additionally conducted with both the **Pd_6M_8** clusters and three selected anionic calixarenes (CX4, CX6, and CX8) to investigate the thermodynamic fingerprint of the supramolecular interaction. The results are summarized in Table 1 (see Figures 3e and S12 for the ITC thermograms). In all cases, the process was enthalpically driven, consistent with the chaotropic effect as dominant driving force.[28,29] In contrast, when "simple" metal cations bind electrostatically to CX*n*, an entropically driven binding is observed.[36] The complex stoichiometry was consistent with a 1:1 complexation pattern (**Pd_6M_8·CX*n***), in line with the fluorescence displacement titrations with **Pd_6Th_8**. Note that phenyl sulfonate, as a monomeric CX*n* model, afforded no heat effect in ITC titrations with **Pd_6M_8** (Figure S13), which reveals the importance of the concave binding site of the calixarene moiety.

The **Pd_6Th_8** affinity (and the enthalpic driving force) for the anionic calixarenes increases with increasing CX*n* size (and flexibility) pointing to a size-matching effect. In contrast, the entropic term is smaller and less diagnostic. The ITC experiments with **Pd_6Ce_8** also provided clear evidence for a strong and enthalpy-driven interaction, but aggregation/precipitation interfered again, in particular at higher concentrations and for CX8, evident through a jump or a bump in the titration curves, which prevented a size- or cluster-dependent quantitative analysis.

Table 1: Association constants (K_a) of cationic mixed-oxo clusters with CX*n* and thermodynamic parameters for complex formation (kcal mol^{-1}).[a]

Host	Guest	K_a [$\times10^5$ M^{-1}]	ΔH°	$T\Delta S^\circ$	ΔG°
CX4	**Pd_6Ce_8**	26	−7.3	1.4	−8.7
	Pd_6Th_8	1.7	−7.8	−1.1	−6.7
CX6	**Pd_6Ce_8**	3.9	−5.9	1.7	−7.6
	Pd_6Th_8	6.5	−8.5	−0.7	−7.8
CX8	**Pd_6Ce_8**	n.a.[b]	n.a.	n.a.	n.a.
	Pd_6Th_8	9.7	−10.4	−2.3	−8.1

[a] 10% Error for K_a and ±0.5 kcal mol^{-1} for ΔH, $T\Delta S$ and ΔG (SD, measured as duplicates). [b] n.a. = not available due to sample aggregation/precipitation.

Subsequently, we attempted to isolate single crystals of the **Pd_6M_8·CX*n*** complexes in order to obtain structural information in the solid-state. In this regard, aqueous solutions of the CX*n* macrocycles (1 mL, 0.002 mmol) were added slowly to aqueous solutions of the **Pd_6M_8** cations (1 mL, 0.002 mmol), and the mixtures were kept at room temperature in an open vial for crystallization. Single crystals suitable for SC-XRD measurement were obtained for the **Pd_6Th_8·CX4** complex after 7 days (Table S1, Figure 3f, Figure S14), whereas for the other systems, precipitation was observed during the same time period. The solid-state structure revealed a **Pd_6Th_8·CX4**[17] complex exhibiting the expected 1:1 complex stoichiometry and conical host conformation of the calixarenes, corroborating the observations in aqueous solution. Within the 1:1 complex, the **Pd_6Th_8** interacts with the CX4 via strong H-bonding interactions (Table S9, Figure S14) through the sulfonate oxygens (H-bond acceptor) and the terminal water molecules coordinated to the Th^{4+} ions (H-bond donor). Each **Pd_6Th_8·CX4** complex further interacts with neighboring complexes in the solid-state via weak H-bonds and C–H···π interactions (Table S9, Table S10, Figure S14) to form the overall supramolecular arrangement. Thus, the SC-XRD study confirmed the nature of the complex as a partial/superficial inclusion complex, and it revealed the proximate, electrostatically favorable positioning of the sulfonato groups towards the cationic oxo-cluster. The host-guest interaction between **Pd_6Th_8** and CX4 has also been studied in the gas-phase using ESI-MS, which indicate the formation of a covalently-linked calixarene complex in the gaseous state (details given in the Supporting Information).

The presence of the cacodylate caps and the ceria and thoria-type components render the two cationic clusters **Pd_6Ce_8** and **Pd_6Th_8** electrochemically inert, unless more negative potentials are applied. However, the Pd^{II} ions eventually undergo irreversible reduction during a voltammetric negative potential scan to form metallic palladium[37] (at −0.2 V, as demonstrated for **Pd_6Ce_8**, Figure S16). The generated Pd^0 sites are expected to behave similarly to Pt and induce redox transitions[38,39] of otherwise highly-inert arsenic oxo species (Figure S17). The existence of reductively-active hydrogen-sorbed species on palladium[40] is of importance as well.

In general, the voltammetric characteristics of **Pd_6Th_8** (Figure 4B) is similar to that of **Pd_6Ce_8** (Figure 4A), except that for **Pd_6Th_8** the reduction of Pd^{II} to Pd^0 is operative at more positive potentials, as compared to **Pd_6Ce_8**, and the generated Pd^0 sites induce reduction of the As-oxo groups within **Pd_6Th_8** (the irreversible reduction peak at about 0.7 V in Figure 4B). Furthermore, due to the presence of interstitial Pd^0 sites, both pre-reduced **Pd_6Ce_8** and **Pd_6Th_8** exhibit electrocatalytic activity toward CO_2-reduction[37,41–43] in the semi-neutral medium of 0.1 mol dm^{-3} phosphate buffer of pH 6.1. Simply judging from the appearance of the well-defined and sound CO_2-reduction peak at the less negative (than typically reported)[37,41,42] potential of −0.3 V

© 2022 The Authors. Angewandte Chemie International Edition published by Wiley-VCH GmbH

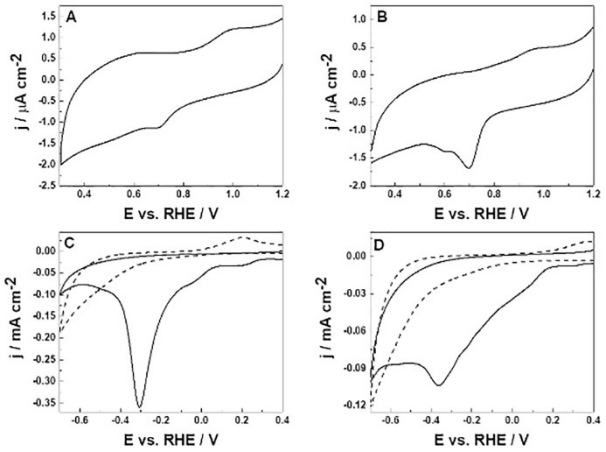

Figure 4. Cyclic voltammetric responses of pre-reduced (i.e., recorded as the second voltammetric cycles after generation of metallic Pd) of a) $\mathbf{Pd_6Ce_8}$ and b) $\mathbf{Pd_6Th_8}$ (Electrolyte, 0.5 mol dm^{-3} H_2SO_4).Voltametric reduction (solid lines) of carbon dioxide (in CO_2-saturated 0.1 mol dm^{-3} phosphate buffer) at pre-reduced c) $\mathbf{Pd_6Ce_8}$ and d) $\mathbf{Pd_6Th_8}$. Dashed lines, which stand for the responses in the CO_2-free solutions, illustrate the Pd-induced hydrogen evolution at potentials lower than −0.2 V. Scan rate, 10 mV s^{-1}.

(Figure 4C) for the pre-reduced $\mathbf{Pd_6Ce_8}$, it can be considered as a potent electrocatalyst for the reduction of CO_2. It is likely that the self-poisoning (with CO) of Pd surfaces becomes less pronounced in such nanoengineered ceria-encapulated Pd clusters. Based on chromatographic analysis performed as described earlier,[37] carbon monoxide and hydrogen (i.e. syngas components) are the main reaction products. The somewhat lower activity of $\mathbf{Pd_6Th_8}$ could be due to the presence of sizeable amounts of the reduced arsenic species in the vicinity of Pd^0 sites (see Supporting Information). Finally, the high electrocatalytic activity of Pd^0 sites within $\mathbf{Pd_6Ce_8}$ can also be seen during the voltammetric oxidation of formic acid. The appearance of a single peak at a potential as low as 0.23 V (Figure S18) is consistent with the direct-oxidation-to-CO_2 (simple dehydrogenation without the intermediate CO adsorbates) mechanism.[40,44,45] Similar to core-shell Pd@CeO_2 catalysts,[46,47] an intimate contact between the central Pd cluster and the surrounding ceria shell can be postulated here. Obviously, the electrogenerated Pd-atomic species are well dispersed with respect to the ceria, and it has been reported before that Pd-nanoparticles smaller than 10 nm induce electrooxidation of formic acid at small positive potentials (<0.3 V).[48]

Conclusion

The use of non-covalent interactions between POMs and various inorganic and organic host materials has recently gained ground as an effective strategy to gain access to molecular assemblies with immense applicability in the area of energy storage, magnetism, sensors, water treatment, and proton conduction.[8i] In addition, the encapsulation of POMs into non-toxic bio-compatible macrocyclic hosts, such as cyclodextrins, can increase the hydrolytic stability of POMs and decrease the inherent cellular toxicity, thereby rendering them useful in medicinal applications as well.[8i] Herein, we have isolated the first two cationic *f*-block ion incorporated palladium(II)-oxo clusters (POCs), $[Pd^{II}{}_6O_{12}M_8\{(CH_3)_2AsO_2\}_{16}(H_2O)_8]^{4+}$ (M = Ce^{IV}, Th^{IV}). To date, only anionic and neutral POCs have been reported in the literature and, therefore, the discovery of cationic POCs represents an important breakthrough in the area of noble-metal-oxo chemistry, especially since it allows the integration of noble-metal ions with *f*-block elements in metal-oxo clusters. The novel compounds have been characterized thoroughly utilizing single-crystal and powder XRD, TGA, IR, XPS, ^{1}H and ^{13}C solution-state NMR and ESI-MS. In addition, we have established here the first case of a discrete, enthalpically-driven supramolecular interaction between large metal-oxo clusters and calixarene macrocycles as based on combined solution, solid-state, and gas-phase studies (^{1}H NMR, fluorescence displacement, ITC, SC-XRD, and ESI-MS). Further, studies on the electrocatalytic performance of $\mathbf{Pd_6Ce_8}$ and $\mathbf{Pd_6Th_8}$ indicated unique enhancement effects toward the electroreduction of CO_2 and electrooxidation of formic acid, which could be attributed to synergies between in situ generated Pd nanoparticles and surrounding ceria or thoria shells. This reaffirms our structural analogy that the two cationic complexes $\mathbf{Pd_6Ce_8}$ and $\mathbf{Pd_6Th_8}$ can be considered as discrete molecular equivalents of nanostructured Pd@ceria or Pd@thoria, respectively.

Acknowledgements

U.K. and W.M.N thank the German Research Council (DFG, KO-2288/29-1, KO-2288/26-1, NA 686/15-1, and NA 686/8-2) and Jacobs University for financial support. A.Ch., I.A.R., and P.J.K. thank the National Science Center (NCN, Poland) for financial support (Opus Project 2018/29/B/ST5/02627). We also thank Emily Schoeneich for help with the fluorescence measurements. The authors declare no competing financial interests. The metal-oxo cluster structural figures were generated by Diamond, Version 3.2 (copyright Crystal Impact GbR). Open Access funding enabled and organized by Projekt DEAL.

Conflict of Interest

The authors declare no conflict of interest.

Data Availability Statement

The data that support the findings of this study are available from the corresponding author upon reasonable request.

© 2022 The Authors. Angewandte Chemie International Edition published by Wiley-VCH GmbH

Keywords: Calixarene · Cerium · Host-Guest Complexes · Palladium · Palladium-Oxo Clusters

[1] a) C. F. Baes, R. E. Mesmer, *The Hydrolysis of Cations*, Krieger, **1986**; b) A. T. Wagner, P. W. Roesky, *Eur. J. Inorg. Chem.* **2016**, 782–791.

[2] a) G.-Y. Yang, D.-G. Huang in *Modern Inorganic Synthetic Chemistry*, 2nd ed., Elsevier, **2017**, chap. 9; b) S. Gross, *J. Mater. Chem.* **2011**, *21*, 15853–15861; c) U. Schubert, *Coord. Chem. Rev.* **2017**, *350*, 61–67; d) S. Gao, *Molecular Nanomagnets and Related Phenomena*, Springer Berlin Heidelberg, Berlin, **2015**.

[3] a) R. Chen, Z.-H. Yan, X.-J. Kong, *ChemPhotoChem* **2020**, *4*, 157–167; b) Q. Han, Y. Ding, *Dalton Trans.* **2018**, *47*, 8180–8188.

[4] a) D. N. Woodruff, R. E. P. Winpenny, R. A. Layfield, *Chem. Rev.* **2013**, *113*, 5110–5148; b) Z. Zheng, *Recent Development in Clusters of Rare Earths and Actinides: Chemistry and Materials*, Springer Berlin Heidelberg, Berlin, **2016**.

[5] W.-H. Fang, L. Zhang, J. Zhang, *Chem. Soc. Rev.* **2018**, *47*, 404–421.

[6] a) R. Cao, *Advanced Structural Chemistry: Tailoring Properties of Inorganic Materials and their Applications*, Wiley-VCH, Weinheim, **2021**; b) Z.-E. Lin, G.-Y. Yang, *Eur. J. Inorg. Chem.* **2011**, 3857–3867; c) Z.-E. Lin, G.-Y. Yang, *Eur. J. Inorg. Chem.* **2010**, 2895–2902; d) C. Falaise, K. Kozma, M. Nyman, *Chem. Eur. J.* **2018**, *24*, 14226–14232; e) Z. Li, L.-D. Lin, H. Yu, X.-X. Li, S.-T. Zheng, *Angew. Chem. Int. Ed.* **2018**, *57*, 15777–15781; *Angew. Chem.* **2018**, *130*, 16003–16007; f) J.-H. Liu, L.-D. Lin, G.-Q. Wang, L.-Y. Li, Y.-Q. Sun, X.-X. Li, S.-T. Zheng, *Chem. Commun.* **2020**, *56*, 10305–10308.

[7] a) M. Pope, Y. Jeannin, M. Fournier, *Heteropoly and Isopoly Oxometalates*, Springer Berlin Heidelberg, Berlin, **1983**; b) M. T. Pope, A. Müller, *Angew. Chem. Int. Ed. Engl.* **1991**, *30*, 34–48; *Angew. Chem.* **1991**, *103*, 56–70; c) M. Amiri, N. P. Martin, C.-L. Feng, J. K. Lovio, M. Nyman, *Angew. Chem. Int. Ed.* **2021**, *60*, 12461–12466; *Angew. Chem.* **2021**, *133*, 12569–12574; d) Z.-K. Zhu, Y.-Y. Lin, H. Yu, X.-X. Li, S.-T. Zheng, *Angew. Chem. Int. Ed.* **2019**, *58*, 16864–16868; *Angew. Chem.* **2019**, *131*, 17020–17024.

[8] a) U. Kortz, *Eur. J. Inorg. Chem.* **2009**, 34; b) A. Dolbecq, E. Dumas, C. R. Mayer, P. Mialane, *Chem. Rev.* **2010**, *110*, 6009–6048; c) N. Mizuno, K. Kamata, *Coord. Chem. Rev.* **2011**, *255*, 2358–2370; d) E. Coronado, C. Giménez-Saiz, C. J. Gómez-García, *Coord. Chem. Rev.* **2005**, *249*, 1776–1796; e) M. T. Pope, A. Müller, *Polyoxometalates: From Platonic Solids to Anti-Retroviral Activity*, Springer Netherlands, Dordrecht, **2012**; f) U. Kortz, A. Müller, J. van Slageren, J. Schnack, N. S. Dalal, M. Dressel, *Coord. Chem. Rev.* **2009**, *253*, 2315–2327; g) D.-L. Long, E. Burkholder, L. Cronin, *Chem. Soc. Rev.* **2007**, *36*, 105–121; h) A. Müller, P. Gouzerh, *Chem. Soc. Rev.* **2012**, *41*, 7431–7463; i) M. Stuckart, K. Y. Monakhov, *Chem. Sci.* **2019**, *10*, 4364–4376.

[9] a) J. W. Döbereiner, *J. Chem. Phys.* **1828**, *54*, 412–426; b) J. C. Goloboy, W. G. Klemperer, *Angew. Chem. Int. Ed.* **2009**, *48*, 3562–3564; *Angew. Chem.* **2009**, *121*, 3614–3616.

[10] a) M. Pley, M. S. Wickleder, *Angew. Chem. Int. Ed.* **2004**, *43*, 4168–4170; *Angew. Chem.* **2004**, *116*, 4262–4264; b) E. V. Chubarova, M. H. Dickman, B. Keita, L. Nadjo, F. Miserque, M. Mifsud, I. W. C. E. Arends, U. Kortz, *Angew. Chem. Int. Ed.* **2008**, *47*, 9542–9546; *Angew. Chem.* **2008**, *120*, 9685–9689; c) N. V. Izarova, N. Vankova, T. Heine, R. Ngo Biboum, B. Keita, L. Nadjo, U. Kortz, *Angew. Chem. Int. Ed.* **2010**, *49*, 1886–1889; *Angew. Chem.* **2010**, *122*, 1930–1933; d) P. Yang, U. Kortz, *Acc. Chem. Res.* **2018**, *51*, 1599–1608; e) N. V. Izarova, N. Vankova, A. Banerjee, G. B. Jameson, T. Heine, F. Schinle, O. Hampe, U. Kortz, *Angew. Chem. Int. Ed.* **2010**, *49*, 7807–7811; *Angew. Chem.* **2010**, *122*, 7975–7980; f) F. Xu, H. N. Miras, R. A. Scullion, D.-L. Long, J. Thiel, L. Cronin, *Proc. Natl. Acad. Sci. USA* **2012**, *109*, 11609.

[11] N. V. Izarova, R. Ngo Biboum, B. Keita, M. Mifsud, I. W. C. E. Arends, G. B. Jameson, U. Kortz, *Dalton Trans.* **2009**, 9385–9387.

[12] Y. Xiang, N. V. Izarova, F. Schinle, O. Hampe, B. Keita, U. Kortz, *Chem. Commun.* **2012**, *48*, 9849–9851.

[13] P. Yang, Y. Xiang, Z. Lin, Z. Lang, P. Jiménez-Lozano, J. J. Carbó, J. M. Poblet, L. Fan, C. Hu, U. Kortz, *Angew. Chem. Int. Ed.* **2016**, *55*, 15766–15770; *Angew. Chem.* **2016**, *128*, 15998–16002.

[14] a) Z. Wang, F.-L. Yang, Y. Yang, Q.-Y. Liu, D. Sun, *Chem. Commun.* **2019**, *55*, 10296–10299; b) Y. Yang, T. Jia, Y.-Z. Han, Z.-A. Nan, S.-F. Yuan, F.-L. Yang, D. Sun, *Angew. Chem. Int. Ed.* **2019**, *58*, 12280–12285; *Angew. Chem.* **2019**, *131*, 12408–12413; c) X.-L. Pei, Y. Yang, Z. Lei, S.-S. Chang, Z.-J. Guan, X.-K. Wan, T.-B. Wen, Q.-M. Wang, *J. Am. Chem. Soc.* **2015**, *137*, 5520–5525; d) E. L.-M. Wong, R. W.-Y. Sun, N. P. Y. Chung, C.-L. S. Lin, N. Zhu, C.-M. Che, *J. Am. Chem. Soc.* **2006**, *128*, 4938–4939; e) S. Chen, W.-H. Fang, L. Zhang, J. Zhang, *Angew. Chem. Int. Ed.* **2018**, *57*, 11252–11256; *Angew. Chem.* **2018**, *130*, 11422–11426; f) H. E. Toma, K. Araki, A. D. P. Alexiou, S. Nikolaou, S. Dovidauskas, *Coord. Chem. Rev.* **2001**, *219–221*, 187–234; g) J. R. Houston, M. M. Olmstead, W. H. Casey, *Inorg. Chem.* **2006**, *45*, 7799–7805; h) M. Ibrahim, M. H. Dickman, A. Suchopar, U. Kortz, *Inorg. Chem.* **2009**, *48*, 1649–1654; i) A. Upadhyay, J. Rajpurohit, M. Kumar-Singh, R. Dubey, A. Kumar Srivastava, A. Kumar, G. Rajaraman, M. Shanmugam, *Chem. Eur. J.* **2014**, *20*, 6061–6070.

[15] a) S. Bhattacharya, U. Basu, M. Haouas, P. Su, M. F. Espenship, F. Wang, A. Solé-Daura, D. H. Taffa, M. Wark, J. M. Poblet, J. Laskin, E. Cadot, U. Kort, *Angew. Chem. Int. Ed.* **2021**, *60*, 3632–3639; *Angew. Chem.* **2021**, *133*, 3676–3683; b) S. Bhattacharya, X. Ma, A. S. Mougharbel, M. Haouas, P. Su, M. F. Espenship, D. H. Taffa, H. Jaensch, A.-J. Bons, T. Stuerzer, M. Wark, J. Laskin, E. Cadot, U. Kortz, *Inorg. Chem.* **2021**, *60*, 17339–17347.

[16] a) G. Hoyez, J. Rousseau, C. Rousseau, S. Saitzek, J. King, P. Á. Szilágyi, C. Volkringer, T. Loiseau, F. Hapiot, E. Monflier, A. Ponchel, *CrystEngComm* **2021**, *23*, 2764; b) L. Barr, P. G. Dumanski, C. J. Easton, J. B. Harper, K. Lee, S. F. Lincoln, A. G. Meyer, J. S. Simpson, *J. Inclusion Phenom. Macrocyclic Chem.* **2004**, *50*, 19–24; c) L. X. Song, L. Bai, X. M. Xu, J. He, S. Z. Pan, *Coord. Chem. Rev.* **2009**, *253*, 1276–1284.

[17] Deposition Numbers 2117327 (for **Pd_6Ce_8**), 2117328 (for **Pd_6Th_8**), and 2117329 (for **Pd_6Th_8·CX4**) contain the supplementary crystallographic data for this paper. These data are provided free of charge by the joint Cambridge Crystallographic Data Centre and Fachinformationszentrum Karlsruhe Access Structures service.

[18] a) G. Chen, F. Rosei, D. Ma, *Nanoscale* **2015**, *7*, 5578; b) S. Zhang, C. Chen, M. Cargnello, P. Fornasiero, R. J. Gorte, G. W. Graham, X. Pan, *Nat. Commun.* **2015**, *6*, 7778; c) J. Ye, D.-G. Cheng, F. Chen, X. Zhan, *Ind. Eng. Chem. Res.* **2019**, *58*, 21972–21982; d) C. M. Y. Yeung, S. C. Tsang, *J. Phys. Chem. C* **2009**, *113*, 6074–6087.

[19] a) W.-X. Tang, P.-X. Gao, *MRS Commun.* **2016**, *6*, 311–329; b) M. Melchionna, P. Fornasiero, *Mater. Today* **2014**, *17*, 349; c) R. K. Behera, C. S. Deo, *J. Phys. Condens. Matter* **2012**, *24*, 215405.

[20] a) S. L. Estes, M. R. Antonio, L. Soderholm, *J. Phys. Chem. C* **2016**, *120*, 5810–5818; b) K. J. Mitchell, K. A. Abboud, G. Christou, *Nat. Commun.* **2017**, *8*, 1445; c) M. C. Wasson, X. Zhang, K.-ichi. Otake, A. S. Rosen, S. Alayoglu, M. D. Krzyaniak, Z. Chen, L. R. Redfern, L. Robison, F. A. Son, Y.

© 2022 The Authors. Angewandte Chemie International Edition published by Wiley-VCH GmbH

Chen, T. Islamoglu, J. M. Notestein, R. Q. Snurr, M. R. Wasielewski, O. K. Farha, *Chem. Mater.* **2020**, *32*, 8522–8529; d) A. Colliard, M. Nyman, *Angew. Chem. Int. Ed.* **2021**, *60*, 7308–7315; *Angew. Chem.* **2021**, *133*, 7384–7391; e) I. L. Malaestean, A. Ellern, S. Baca, P. Kögerler, *Chem. Commun.* **2012**, *48*, 1499–1501; f) K. E. Knope, R. E. Wilson, M. Vasiliu, D. A. Dixon, L. Soderholm, *Inorg. Chem.* **2011**, *50*, 9696–9704; g) K. E. Knope, M. Vasiliu, D. A. Dixon, L. Soderholm, *Inorg. Chem.* **2012**, *51*, 4239–4249.

[21] a) J. F. Moulder, W. F. Stickle, P. E. Sobol, K. D. Bomben, *Handbook of X-ray Photoelectron Spectroscopy* (Ed.: J. Chastain), Perkin-Elmer Corp., Eden Prairie, **1992**; b) "Ag Foil by XPS": G. B. Hoflund, J. F. Weaver, W. S. Epling, *Surf. Sci. Spectra* **1994**, *3*, 151–156; c) Y. A. Teterin, A. Y. Teterin, A. M. Lebedev, I. O. Utkin, *J. Electron Spectrosc. Relat. Phenom.* **1998**, *88–91*, 275–279; d) E. Bêche, P. Charvin, D. Perarnau, S. Abanades, G. Flamant, *Surf. Interface Anal.* **2008**, *40*, 264–267; e) S. Dash, A. Singh, P. K. Ajikumar, H. Subramanian, M. Rajalakshmi, A. K. Tyagi, A. K. Arora, S. V. Narasimhan, B. Raj, *J. Nucl. Mater.* **2002**, *303*, 156–168.

[22] a) L. Gianelli, V. Amendola, L. Fabbrizzi, P. Pallavicini, G. G. Mellerio, *Rapid Commun. Mass Spectrom.* **2001**, *15*, 2347–2353; b) H. Lavanant, H. Virelizier, Y. Hoppilliard, *J. Am. Soc. Mass Spectrom.* **1998**, *9*, 1217–1221; c) H. Waska, A. Koschinsky, T. Dittmar, *Front. Mar. Sci.* **2016**, *3*, 119.

[23] a) Y. Wu, R. Shi, Y.-L. Wu, J. M. Holcroft, Z. Liu, M. Frasconi, M. R. Wasielewski, H. Li, J. F. Stoddart, *J. Am. Chem. Soc.* **2015**, *137*, 4111–4118; b) J. Szejtli, *Chem. Rev.* **1998**, *98*, 1743–1753.

[24] a) M. A. Moussawi, M. Haouas, S. Floquet, W. E. Shepard, P. A. Abramov, M. N. Sokolov, V. P. Fedin, S. Cordier, A. Ponchel, E. Monflier, J. Marrot, E. Cadot, *J. Am. Chem. Soc.* **2017**, *139*, 14376–14379; b) M. A. Moussawi, N. Leclerc-Laronze, S. Floquet, P. A. Abramov, M. N. Sokolov, S. Cordier, A. Ponchel, E. Monflier, H. Bricout, D. Landy, M. Haouas, J. Marrot, E. Cadot, *J. Am. Chem. Soc.* **2017**, *139*, 12793–12803.

[25] a) S. Yao, C. Falaise, A. A. Ivanov, N. Leclerc, M. Hohenschutz, M. Haouas, D. Landy, M. A. Shestopalov, P. Bauduin, E. Cadot, *Inorg. Chem. Front.* **2021**, *8*, 12–25; b) P. Su, A. J. Smith, J. Warneke, J. Laskin, *J. Am. Soc. Mass Spectrom.* **2019**, *30*, 1934–1945; c) Y. Fan, S. Lu, J. Cao, *Int. J. Mass Spectrom.* **2019**, *435*, 163–167; d) L. Ni, H. Li, H. Xu, C. Shen, R. Liu, J. Xie, F. Zhang, C. Chen, H. Zhao, T. Zuo, G. Diao, *ACS Appl. Mater. Interfaces* **2019**, *11*, 38708–38718.

[26] C. Falaise, M. A. Moussawi, S. Floquet, P. A. Abramov, M. N. Sokolov, M. Haouas, E. Cadot, *J. Am. Chem. Soc.* **2018**, *140*, 11198–11201.

[27] A. A. Ivanov, T. N. Pozmogova, A. O. Solovieva, T. S. Frolova, O. I. Sinitsyna, O. V. Lundovskaya, A. R. Tsygankova, M. Haouas, D. Landy, E. Benassi, L. V. Shestopalova, C. Falaise, E. Cadot, M. A. Shestopalov, P. A. Abramov, M. N. Sokolov, *Chem. Eur. J.* **2020**, *26*, 7479–7485.

[28] a) B. Naskar, O. Diat, V. Nardello-Rataj, P. Bauduin, *J. Phys. Chem. C* **2015**, *119*, 20985–20992; b) K. I. Assaf, M. S. Ural, F. Pan, T. Georgiev, S. Simova, K. Rissanen, D. Gabel, W. M. Nau, *Angew. Chem. Int. Ed.* **2015**, *54*, 6852–6856; *Angew. Chem.* **2015**, *127*, 6956–6960.

[29] K. I. Assaf, W. M. Nau, *Angew. Chem. Int. Ed.* **2018**, *57*, 13968–13981; *Angew. Chem.* **2018**, *130*, 14164–14177.

[30] a) Y.-C. Pan, X.-Y. Hu, D.-S. Guo, *Angew. Chem. Int. Ed.* **2021**, *60*, 2768–2794; *Angew. Chem.* **2021**, *133*, 2800–2828; b) R. Kumar, A. Sharma, H. Singh, P. Suating, H. S. Kim, K. Sunwoo, I. Shim, B. C. Gibb, J. S. Kim, *Chem. Rev.* **2019**, *119*, 9657–9721; c) E. S. Español, M. M. Villamil, *Biomol. Eng.* **2019**, *9*, 90; d) S. Kumar, S. Chawla, M. C. Zou, *J. Inclusion Phenom. Macrocyclic Chem.* **2017**, *88*, 129–158; e) D. M. Homden, C. Redshaw, *Chem. Rev.* **2008**, *108*, 5086–5130.

[31] H. Bakirci, A. L. Koner, W. M. Nau, *J. Org. Chem.* **2005**, *70*, 9960–9966.

[32] H. Bakirci, T. Schwarzlose, A. L. Koner, W. M. Nau, *Chem. Eur. J.* **2006**, *12*, 4799–4807.

[33] C. D. Gutsche, L. J. Bauer, *J. Am. Chem. Soc.* **1985**, *107*, 6052–6059.

[34] R. N. Dsouza, U. Pischel, W. M. Nau, *Chem. Rev.* **2011**, *111*, 7941–7980.

[35] D.-S. Guo, V. D. Uzunova, X. Su, Y. Liu, W. M. Nau, *Chem. Sci.* **2011**, *2*, 1722–1734.

[36] a) H. Bakirci, A. L. Koner, W. M. Nau, *Chem. Commun.* **2005**, 5411–5413; b) V. Francisco, A. Piñeiro, W. M. Nau, L. García-Río, *Chem. Eur. J.* **2013**, *19*, 17809–17820.

[37] A. Wadas, A. Gorczynski, I. A. Rutkowska, E. Seta-Wiaderek, E. Szaniawska, M. Kubicki, A. Lewera, M. Gorzkowski, A. Januszewska, R. Jurczakowski, B. Palys, V. Patroniak, P. J. Kulesza, *Electrochim. Acta* **2021**, *388*, 138550.

[38] J. A. Cox, I. A. Rutkowska, P. J. Kulesza, *J. Electrochem. Soc.* **2020**, *167*, 037565.

[39] W. B. Postek, I. A. Rutkowska, J. A. Cox, P. J. Kulesza, *Electrochim. Acta* **2019**, *319*, 499–510.

[40] I. A. Rutkowska, D. Marks, C. Perruchot, M. Jouini, P. J. Kulesza, *Colloids Surf. A* **2013**, *439*, 200–206.

[41] D. Gao, H. Zhou, F. Cai, J. Wang, G. Wang, X. Bao, *ACS Catal.* **2018**, *8*, 1510–1519.

[42] Y. Zhao, X. Tan, W. Yang, C. Jia, X. Chen, W. Ren, S. C. Smith, C. Zhao, *Angew. Chem. Int. Ed.* **2020**, *59*, 21493–21498; *Angew. Chem.* **2020**, *132*, 21677–21682.

[43] P. J. Kulesza, I. A. Rutkowska, *Electrochem. Soc. Interface* **2020**, *29*, 67–72.

[44] W.-L. Qu, Z.-B. Wang, X.-L. Sui, D.-M. Gu, G.-P. Yin, *Fuel Cells* **2013**, *13*, 149–157.

[45] I. A. Rutkowska, *Aust. J. Chem.* **2016**, *69*, 394–402.

[46] M. Cargnello, J. J. Delgado Jaén, J. C. Hernández Garrido, K. Bakhmutsky, T. Montini, J. J. Calvino Gámez, R. J. Gorte, P. Fornasiero, *Science* **2012**, *337*, 713–717.

[47] L. Adijanto, D. A. Bennett, C. Chen, A. S. Yu, M. Cargnello, P. Fornasiero, R. J. Gorte, J. M. Vohs, *Nano Lett.* **2013**, *13*, 2252–2257.

[48] W. Ju, R. Valiollahi, R. Ojani, O. Schneider, U. Stimming, *Electrocatalysis* **2016**, *7*, 149–158.

Manuscript received: February 27, 2022
Accepted manuscript online: April 5, 2022
Version of record online: April 27, 2022

© 2022 The Authors. Angewandte Chemie International Edition published by Wiley-VCH GmbH